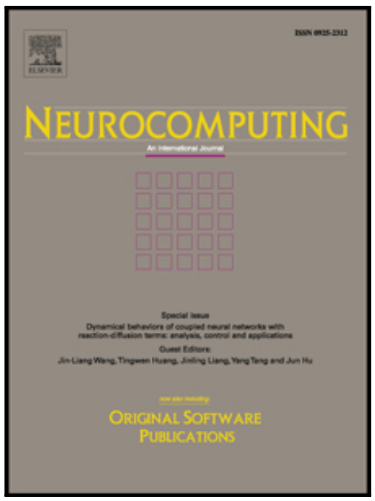

Verification and predicting temperature and humidity in a solar greenhouse based on convex bidirectional extreme learning machine algorithm

Weidong Zou, Fenxi Yao, Baihai Zhang, Chaoxing He, Zixiao Guan

PII: S0925-2312(17)30518-0
DOI: 10.1016/j.neucom.2017.03.023
Reference: NEUCOM 18244

To appear in: *Neurocomputing*

Received date: 19 January 2016
Revised date: 24 January 2017
Accepted date: 9 March 2017

Please cite this article as: Weidong Zou, Fenxi Yao, Baihai Zhang, Chaoxing He, Zixiao Guan, Verification and predicting temperature and humidity in a solar greenhouse based on convex bidirectional extreme learning machine algorithm, *Neurocomputing* (2017), doi: 10.1016/j.neucom.2017.03.023

Verification and predicting temperature and humidity in a solar greenhouse based on convex bidirectional extreme learning machine algorithm☆

Weidong Zou[a], Fenxi Yao[a,*], Baihai Zhang[a], Chaoxing He[b], Zixiao Guan[a]

[a]*School of Automation, Beijing Institute of Technology, Beijing 100081, PR China*
[b]*The Institute of Vegetables and Flowers, Chinese Academy of Agricultural Sciences, Beijing 100081, PR China*

Abstract

Predictions regarding the solar greenhouse temperature and humidity are important because they play a critical role in greenhouse cultivation. On account of this, it is important to set up a predictive model of temperature and humidity that would precisely predict the temperature and humidity, reducing potential financial losses. This paper presents a novel temperature and humidity prediction model based on convex bidirectional extreme learning machine (CB-ELM). Simulation results show that the convergence rate of the bidirectional extreme learning machine (B-ELM) can further be improved while retaining the same simplicity, by simply recalculating the output weights of the existing nodes based on a convex optimization method when a new hidden node is randomly added. The performance of the CB-ELM model is compared with other modeling approaches by applying it to predict solar greenhouse temperature and humidity. The experiment results show that the CB-ELM model predictions are more accurate than those of the B-ELM, Back Propagation Neural Network (BPNN), Support Vector Machine (SVM), and Radial Basis Function (RBF). Therefore, it can be considered as a suitable and effective method for predicting the solar greenhouse temperature and humidity.

Keywords: Solar greenhouse, support vector machine, radial basis Function, convex bidirectional extreme learning machine

1. Introduction

The solar greenhouse covered with plastic and a thermal blanket is a very complex dynamic system [1-3]. It extends the growing season in cold climatic conditions, producing greenhouse crops year round. As such, solar greenhouses

*Corresponding author
Email address: yaofenxi1964@163.com (Fenxi Yao)

must provide good environmental conditions for greenhouse crop growth, especially by maintaining adequate temperature and humidity. Greenhouse crops exposed to low or high temperature and humidity may lead to mass death or fungal diseases. Therefore, to reduce financial losses, it is crucial to set up a precise predictive model of both temperature and humidity in the solar greenhouse [4]. Many modeling methods have been proposed for the solar greenhouse, including mechanism modeling and black-box modeling. The black-box model is based upon input and output data, and is suitable for both linear and nonlinear modeling. The mechanism model provides a clear physical explanation of the solar greenhouse [5]. Generally, the dynamics of air temperature and humidity in greenhouses are described in many ways, such as classical Albright's [6] model:

$$\frac{dT_{in}}{dt} = \frac{1}{\rho C_p V}(q_{heater} + I_{in} - \lambda q_{fog}) - \frac{\varphi_{vent}}{V}(T_{in} - T_{out}) - \frac{K_e}{\rho C_p V}(T_{in} - T_{out}) \quad (1)$$

$$\frac{dH_{in}}{dt} = \frac{1}{V} q_{fog} + \frac{1}{V} E(I_{in}, H_{in}) - \frac{\varphi_{vent}}{V}(H_{in} - H_{out}) \quad (2)$$

Where T_{in} is indoor temperature (°C), T_{out} is outdoor temperature (°C), V is greenhouse volume (m^3), K_e is heat transfer coefficient ($W \cdot K^{-1}$), ρ is air density ($kg{\cdot}m^{-3}$), C_p is specific heat of air ($J{\cdot}(kg{\cdot}K)^{-1}$), q_{heater} is heat provided by the greenhouse heater (W), I_{in} is intercepted solar radiant energy (W), q_{fog} is water capacity of fog system ($kg(m^2 \cdot K)^{-1}$), λ is latent heat of vaporization ($J \cdot g^{-1}$), φ_{vent} is ventilation rate ($m^3 \cdot s^{-1}$), H_{in} is indoor temperature (%), H_{out} is outdoor temperature (%), E is evapotranspiration rate of the plants.

The main shortcomings of Albright's model can be summarized as follows:

(1) It is too simple to accurately reflect the relationships between greenhouse environment and crop growing process;

(2) Carbon dioxide concentration, which is an important environmental factor to affect photosynthesis, is not included in Albright's model.

Neural networks, which can model nonlinear systems, have been applied to solar greenhouse environment modeling. Ferreira et al. [7] use the adequacy of radial basis function neural networks to model the inside air temperature of a hydroponic greenhouse as a function of the outside air temperature and solar radiation, as well as the inside relative humidity. For modeling the internal greenhouse humidity in winter of North China, Fen He et al. [8] proposed a BPNN based on principal component analysis (PCA). In order to create clusters, the ART2 classifier is used to decompose a database of a greenhouse. When the clusters are formed, the Elman neural network can be trained to model each cluster in order to achieve control over the considered greenhouse through multiple neural networks [9]. Wang et al. [10] used online sparse least-squares support vector machines regression with linear kernel function to model the greenhouse environment. Amine Trabelsi et al. [11] proposed a study on the application of the Takagi-Sugeno (TS) fuzzy models to the identification problem of greenhouse modeling. Based on the BP neural network model, He et al. [12]

analyze the influencing factors importance of inside air humidity which the inside temperature, outside temperature and humidity, open ration of sunshade curtain, wind speed, solar radiation and open angle of top and side vent. In order research the change trends of relative humidity in northern greenhouse, Xu et al. [13] propose a simulation and prediction model of humidity factors based on RBF neural network with Gaussian radial basis function.

However, all of the parameters of conventional neural networks (such as BPNN [14], RBF [15], and Elman neural network [16]) are tuned iteratively by using slow gradient-based learning algorithms, making the learning speed of neural network far slower than required. Huang et al. [17] proposed simple and efficient learning steps, both with increased network architecture and incremental extreme learning machine (I-ELM). The method generates parameters of a hidden node randomly; it is easy to get the output weight by training the single hidden layer feedforward neural networks (SLFNs). This makes the selection of the weights of the hidden neurons relatively fast in the case of SLFNs. Hence, the overall computational time for the model structure selection and actual training is often reduced by several hundred times than found in some conventional methods such as BP, RBF, and Elman neural network. Based on I-ELM, several methods with the mechanism of growth hidden nodes are proposed, such as convex I-ELM [18], enhanced I-ELM [19], optimal pruned ELM [20], error-minimized ELM [21], two-stage ELM [22], and bidirectional ELM [23].

For incremental ELM methods such as I-ELM, CI-ELM, EM-ELM, and OP-ELM, Huang et al. proved in [17] that with increasing hidden nodes, the residual error of SLFNs decreased and bounded below by zero. This result makes it easy for the user to determine the network structure by adding hidden nodes one by one until achieving the expected training accuracy. However, experimental results show that the learning time of incremental ELM methods increase many times compared with ELM. It is because I-ELM calculates n output weights one by one when n hidden nodes are used. But ELM only calculates these n output weights once when n hidden nodes are used.

To further improved the generalization performance of I-ELM, CB-ELM is proposed. Compared with the existing work already reported in literature, the contributions and novelty of this paper reside in the following two aspects: (1) a relationship was found between the network output error and the network output weights in the proposed convex bidirectional extreme learning machine (CB-ELM); and (2) CB-ELM was used to forecast temperature and humidity in solar greenhouse.

2. Proposed Convex Bidirectional ELM method

In this section, we first prove that CB-ELM with sine or sigmoid activation function can universally approximate any continuous target functions in Section 2.1. Then we discuss the learning effectiveness of CB-ELM in Section 2.2. Finally, the algorithm of CB-ELM is given in Section 2.3.

2.1. Convex bidirectional ELM Methods

Lemma 2.1 ([18]) Given a SLFN with nonconstant piecewise continuous hidden nodes $\mathbf{H}(\mathbf{x}, \mathbf{a}, b)$, then for any continuous target function f and any function sequence $\mathbf{H}_n^r(\mathbf{x}) = \mathbf{H}(\mathbf{x}, \mathbf{a}_n, b_n)$ randomly generated based on any continuous sampling distribution, $\lim_{n\to\infty} \|f-(1-\beta_n)f_{n-1}+\beta_n g_n\| = 0$ holds with probability 1 if

$$\beta_n = \frac{< e_{n-1}, \mathbf{H}_n^r - f_{n-1} >}{\|\mathbf{H}_n^r - f_{n-1}\|^2} \tag{3}$$

Where $e_n = f - f_n$ denotes the residual error function for the current network f_n with n hidden nodes.

Theorem 2.2 Given a SLFN with any bounded nonconstant piecewise continuous function $\mathbf{H} : \mathbf{R} \to \mathbf{R}$ for additive hidden nodes, for any continuous target function f, randomly generated function sequence $\mathbf{H}_{2n+1}^r$, and obtained error feedback function sequence $\mathbf{H}_{2n}^e$, $n \in Z$, $\lim_{n\to\infty} \|f - (1-\beta_{2n-1})(1-\beta_{2n})f_{2n-2} - (1-\beta_{2n})\beta_{2n-1}H_{2n-1} - \beta_{2n}H_{2n}^e\| = 0$ holds with probability 1 if

$$\mathbf{H}_{2n}^e = e_{2n-1}(\beta_{2n-1})^{-1} + f_{2n-1} \tag{4}$$

$$\beta_{2n} = \frac{\langle e_{2n-1}, \mathbf{H}_{2n}^e - f_{2n-1} \rangle}{\|\mathbf{H}_{2n}^e - f_{2n-1}\|^2} \tag{5}$$

$$\beta_{2n+1} = \frac{\langle e_{2n}, \mathbf{H}_{2n+1}^r - f_{2n} \rangle}{\left\|H_{2n+1}^r - f_{2n}\right\|^2}. \tag{6}$$

Proof. We first prove that the sequence $\|e_{2n}\|$ is decreasing and bounded below by zero and it converges. Then we further prove $\lim_{n\to\infty} \|e_{2n}\| = 0$.

(a) Let $\mathbf{H}_L = \mathbf{H}_1(\mathbf{a}_1, ..., \mathbf{a}_L, b_1, ..., b_L, \mathbf{x}_1, ..., \mathbf{x}_N)$ denotes the hidden layer output matrix. We have $e_{2n-1} = f - \left[\mathbf{H}_1^r, \mathbf{H}_2^e, ..., \mathbf{H}_{2n-1}^r\right] \cdot [\beta_1, \beta_2, ..., \beta_{2n-1}]^T$. Let $\Delta = \|e_{2n-1}\|^2 - \|e_{2n}\|^2$, since $\|e_{2n}\| = \|e_{2n-1} - \beta_{2n}(\mathbf{H}_{2n}^e - f_{2n-1})\|$, we have

$$\begin{aligned} \Delta &= \|e_{2n-1}\|^2 - \|e_{2n-1} - \beta_{2n}(\mathbf{H}_{2n}^e - f_{2n-1})\|^2 \\ &= 2\beta_{2n} \langle e_{2n-1}, \mathbf{H}_{2n}^e - f_{2n-1} \rangle - \beta_{2n}^2 \|\mathbf{H}_{2n}^e - f_{2n-1}\|^2 \\ &= \beta_{2n}^2 \|\mathbf{H}_{2n}^e - f_{2n-1}\|^2 \geq 0. \end{aligned} \tag{7}$$

In [17], Huang et al. have proved that $\|e_{2n}\|^2 - \left\|e_{2n} - \mathbf{H}_{2n+1}^r \beta_{2n+1}\right\|^2 \geq 0$, thus $\|e_{2n}\| \geq \|e_{2n+1}\|$. We have $\|e_{2n-1}\| \geq \|e_{2n}\| \geq \|e_{2n+1}\|$, so the sequence $\{\|e_n\|\}$ is decreasing and bounded below by zero and $\{\|e_n\|\}$ is convergent.

(b) Seen from the proof of the original I-ELM [17], the sequence $\{\|e_n\|\}$ converges to zero as long as the three sufficient conditions below are satisfied:

(1)$span\left\{\mathbf{H}(\mathbf{x}, \mathbf{a}, b) : (\mathbf{a}, b) \in \mathbf{R}^d \times R\right\}$ is dense in L^2;

(2)$e_{2n} \perp (e_{2n-1} - e_{2n})$;

(3)$\mathbf{H}$ is a nonconstant piecewise continuous function.

Since conditions (1) and (3) have been given as the preconditions of the theorem, in order to prove $\lim_{n\to\infty}\|e_{2n}\|=0$, we need to prove $e_{2n}\perp(e_{2n-1}-e_{2n})$. Since $\|e_{2n}\|=\|e_{2n-1}-\beta_{2n}(\mathbf{H}_{2n}^{e}-f_{2n-1})\|$, we have

$$\begin{aligned}&\langle e_{2n},\mathbf{H}_{2n}^{e}-f_{2n-1}\rangle\\&=\langle e_{2n-1}-\beta_{2n}(\mathbf{H}_{2n}^{e}-f_{2n-1}),\mathbf{H}_{2n}^{e}-f_{2n-1}\rangle\\&=\langle e_{2n-1},\mathbf{H}_{2n}^{e}-f_{2n-1}\rangle-\beta_{2n}\|\mathbf{H}_{2n}^{e}-f_{2n-1}\|^{2}=0.\end{aligned}\tag{8}$$

According to formula (8), we further have

$$\begin{aligned}&\langle e_{2n},e_{2n-1}-e_{2n}\rangle\\&=\langle e_{2n},e_{2n}+\beta_{2n}(\mathbf{H}_{2n}^{e}-f_{2n-1})\rangle-\|e_{2n}\|^{2}\\&=\|e_{2n}\|^{2}-\beta_{2n}\langle e_{2n},\mathbf{H}_{2n}^{e}-f_{2n-1}\rangle-\|e_{2n}\|^{2}=0,\end{aligned}\tag{9}$$

which means $e_{2n}\perp(e_{2n-1}-e_{2n})$. This completes the proof of theorem 2.2.

Remark 1: Theorem 2.2 is established on the basis of reference 23 with a convex optimization method.

Lemma 2.3 ([23]) Given a sigmoid or sine activation function $h:\mathbf{R}\to\mathbf{R}$. Given an error feedback function sequence $\mathbf{G}_{2n}^{e}(\mathbf{x},\mathbf{a},b)$, and $\mathbf{G}_{2n}^{e}=e_{2n-1}(\beta_{2n-1})^{-1}$. If the activation function h is sin or cosine, given a normalized function $u:\mathbf{R}\to[0,1]$. If the activation function h is sigmoid, given a normalized function $u:\mathbf{R}\to(0,1]$. Then for any continuous target function f, the randomly generated function sequence $\mathbf{G}_{2n+1}^{r}$, $\lim_{n\to\infty}\left\|f-\left(\mathbf{G}_{1}^{r}\beta_{1}+\hat{\mathbf{G}}_{2}^{e}(\hat{\mathbf{a}}_{2},\hat{b}_{2})\beta_{2}+...+\mathbf{G}_{2n-1}^{r}\beta_{2n-1}+\hat{\mathbf{G}}_{2n}^{e}(\hat{\mathbf{a}}_{2n},\hat{b}_{2n})\beta_{2n}\right)\right\|=0$ holds with probability 1 if

$$\hat{\mathbf{a}}_{2n}=h^{-1}(u(\mathbf{G}_{2n}^{e}))\cdot\mathbf{x}^{-1}\tag{10}$$

$$\hat{b}_{2n}=\sqrt{mse(h^{-1}(u(\mathbf{G}_{2n}^{e}))\cdot\mathbf{x}^{-1}-\hat{\mathbf{a}}_{2n}\cdot\mathbf{x})}\tag{11}$$

$$\hat{\mathbf{G}}_{2n}^{e}=u^{-1}(h(\hat{\mathbf{a}}_{2n}\cdot\mathbf{x}+\hat{b}_{2n})).\tag{12}$$

Where h^{-1} and u^{-1} represent its reverse function respectively. If h is a sine activation function, $h^{-1}(\cdot)=\arcsin(\cdot)$. If h is a sigmoid activation function, $h^{-1}(\cdot)=-\ln(\frac{1}{(\cdot)}-1)$.

According to formula (4) and Lemma 2.3, if

$$\hat{\mathbf{a}}_{2n}=h^{-1}(u(\mathbf{H}_{2n}^{e}))\cdot\mathbf{x}^{-1}\tag{13}$$

$$\hat{b}_{2n}=\sqrt{mse(h^{-1}(u(\mathbf{H}_{2n}^{e}))\cdot\mathbf{x}^{-1}-\hat{\mathbf{a}}_{2n}\cdot\mathbf{x})}\tag{14}$$

$$\hat{\mathbf{H}}_{2n}^{e}=u^{-1}(h(\hat{\mathbf{a}}_{2n}\cdot\mathbf{x}+\hat{b}_{2n}))\tag{15}$$

Where h^{-1} and u^{-1} represent its reverse function respectively. If h is a sine activation function, $h^{-1}(\cdot)=\arcsin(\cdot)$. If h is a sigmoid activation function, $h^{-1}(\cdot)=-\ln(\frac{1}{(\cdot)}-1)$.

We have $\lim_{n\to\infty}\left\|f-\left(\mathbf{H}_1^r\beta_1+\hat{\mathbf{H}}_2^e(\hat{\mathbf{a}}_2,\hat{b}_2)\beta_2+...+\mathbf{H}_{2n-1}^r\beta_{2n-1}+\hat{\mathbf{H}}_{2n}^e(\hat{\mathbf{a}}_{2n},\hat{b}_{2n})\beta_{2n}\right)\right\|=0$.

Remark 2: According to formula (4), formula (7) can be rewritten as

$$\|e_{2n-1}\|^2-\|e_{2n}\|^2=\beta_{2n}^2\|\mathbf{H}_{2n}^e-f_{2n-1}\|^2=\|e_{2n-1}\|^2\frac{\beta_{2n}^2}{\beta_{2n-1}^2}. \tag{16}$$

Thus, we have

$$\frac{\|e_{2n}\|^2}{\|e_{2n-1}\|^2}+\frac{\beta_{2n}^2}{\beta_{2n-1}^2}=1. \tag{17}$$

Formula(17) shows a relationship between the network output error and the network output weights. This result is the same as that of [21].

2.2. Learning effectiveness of CB-ELM

In this section, we analyze the learning effectiveness of CB-ELM.

According to formula (4), we have

$$\frac{1}{|\beta_{2n-1}|}=\frac{\|\mathbf{H}_{2n}^e-f_{2n-1}\|}{\|e_{2n-1}\|}. \tag{18}$$

If set $\tau_{2n-1}=|\beta_{2n-1}|-|\beta_{2n}|$, we have

$$\frac{|\beta_{2n}|}{|\beta_{2n-1}|}=1-\frac{\tau_{2n-1}}{|\beta_{2n-1}|}. \tag{19}$$

Considering formula (17) and formula (19), we have

$$\frac{\|e_{2n}\|^2}{\|e_{2n-1}\|^2}+\left(1-\frac{\tau_{2n-1}}{|\beta_{2n-1}|}\right)^2=1 \tag{20}$$

and

$$\frac{\|e_{2n}\|^2}{\|e_{2n-1}\|^2}+\frac{\tau_{2n-1}^2}{\beta_{2n-1}^2}=2\frac{\tau_{2n-1}}{|\beta_{2n-1}|}. \tag{21}$$

According to formula (18) and formula (21), we get

$$\frac{\|e_{2n}\|^2}{\|e_{2n-1}\|^2}+\frac{\tau_{2n-1}^2\|\mathbf{H}_{2n}^e-f_{2n-1}\|^2}{\|e_{2n-1}\|^2}=2\frac{\tau_{2n-1}\|\mathbf{H}_{2n}^e-f_{2n-1}\|}{\|e_{2n-1}\|}. \tag{22}$$

We further have

$$\begin{aligned}&\tau_{2n-1}^2\|\mathbf{H}_{2n}^e-f_{2n-1}\|^2-2\tau_{2n-1}\|e_{2n-1}\|\|\mathbf{H}_{2n}^e-f_{2n-1}\|+\|e_{2n-1}\|^2\\&=\|e_{2n-1}\|^2-\|e_{2n}\|^2.\end{aligned} \tag{23}$$

According to formula(9), we have

$$\langle e_{2n},e_{2n-1}\rangle=\|e_{2n}\|^2. \tag{24}$$

According to theorem 2.2, we have

$$\begin{aligned} &\|e_{2n-1} - e_{2n}\|^2 \\ &= \|e_{2n-1}\|^2 + \|e_{2n}\|^2 - 2\langle e_{2n-1}, e_{2n}\rangle \\ &= \|e_{2n-1}\|^2 - \|e_{2n}\|^2. \end{aligned} \tag{25}$$

Considering formula (23) and formula (25), we have

$$\|e_{2n-1}\| - \tau_{2n-1}\|\mathbf{H}_{2n}^e - f_{2n-1}\| = \|e_{2n-1} - e_{2n}\|. \tag{26}$$

In [17], Huang et al. have proved that

$$\|e_{2n-1}\| - \|e_{2n}\| = \|e_{2n-1} - e_{2n}\| \tag{27}$$

thus, from formula (26) and formula (27), we have

$$\|e_{2n-1}\| - \tau_{2n-1}\|\mathbf{H}_{2n}^e - f_{2n-1}\| = \|e_{2n-1}\| - \|e_{2n}\|. \tag{28}$$

Considering formula (18) and formula (28), we have

$$\frac{\|e_{2n}\|}{\|e_{2n-1}\|} = \frac{\tau_{2n-1}}{|\beta_{2n-1}|} \tag{29}$$

and

$$\frac{\tau_{2n-1}^2}{|\beta_{2n-1}|^2} + \left(1 - \frac{\tau_{2n-1}}{|\beta_{2n-1}|}\right)^2 = 1. \tag{30}$$

We get the solution $\frac{\tau_{2n-1}}{|\beta_{2n-1}|} = 1$ and $\frac{\tau_{2n-1}}{|\beta_{2n-1}|} = 0$.

According to theorem 2.2, we have $\|e_{2n-1}\| > \|e_{2n}\|$, thus, we have $\frac{\|e_{2n}\|}{\|e_{2n-1}\|} = \frac{\tau_{2n-1}}{|\beta_{2n-1}|} \neq 1$. $\frac{\|e_{2n}\|}{\|e_{2n-1}\|} = \frac{\tau_{2n-1}}{|\beta_{2n-1}|}$ is only equal to 0.

Remark 3: When an SLFN with two hidden nodes is trained by CB-ELM, it shows that $\|e_1\| - \|e_2\| > 0$, $\|e_1\| \neq 0$. According to formula (29) and formula (30), we get $\frac{\|e_2\|}{\|e_1\|} = 0$ and $\|e_2\| = 0$. Thus, in theory, CB-ELM with two hidden nodes can reduce network output error e to 0. This result is the same as that of [23].

2.3. Pseudo-Code for CB-ELM Method

The proposed CB-ELM for SLFN can be summarized as follows: Algorithm CB-ELM. Given a training set $\{(\mathbf{x}_i, t_i)\}_{i=1}^N \subset \mathbf{R}^n \times \mathbf{R}$, activation function $\mathbf{H}(\mathbf{a}, \mathbf{x}, b)$, the continuous target function f and maximum number of hidden nodes $L_{\max}$, the expected learning accuracy ε,

Step Initialization: Let the number of hidden nodes $L = 0$ and the residual error $E = t$, where $t = [t_1, ..., t_N]$.

Learning step: While $L < L_{\max}$ and $\|E\| > \varepsilon$, increase the number of hidden nodes L by 1:$L = L + 1$. If $L \in \{2n + 1, n \in z\}$ then

(a) Randomly assign hidden node of parameters $(\mathbf{a}_L, b_L)$ for new hidden node L.

(b) Calculate the output weight β_L for the new hidden node :

$$\beta_L = \frac{E \cdot [E - (F - H_L)]^T}{[E - (F - H_L)]\,[E - (F - H_L)]^T} \tag{31}$$

(c) Calculate the residual error after adding the new hidden node L : $E = (1 - \beta_L)\,E - \beta_L\,(F - H_L)$

End if.

If $L \in \{2n, n \in z\}$ then

(a) Calculate the error feedback function sequence H_L:

$$H_L = \frac{E}{\beta_L} + F \tag{32}$$

(b) Calculate the input weight a_L, bias b_L and update H_L for the new hidden node L based on (13), (14) and (15);

(c) Calculate the output weight β_L for the new hidden node according to (3);

(d) Calculate the residual error after adding the new hidden node L : $E = (1 - \beta_L)\,E - \beta_L\,(F - H_L)$.

End if

End while

3. Experimental verification

For testing the generalization performance of CB-ELM, in this section, we test it on 8 regression problems which are collected from the University of California at Irvine (UCI) Machine Learning Repository and data of solar greenhouse temperature and humidity. The simulations are conducted in Matlab 2010a running on Windows 7 with at 4 GB of memory and two Dual-Core E5300 (2.60 GHZ) processors. Learning algorithms are tested with I-ELM, CI-ELM, B-ELM, SVM, BP, RBF and CB-ELM.

3.1. Experiments of regression problems

Eight regression datasets are selected for the experiments and described in Table 1. We preprocess all datasets in the same way.

CB-ELM, B-ELM, I-ELM and CI-ELM are compared in eight regression problems. The number of hidden nodes is selected from 1 to 30 by step 1. Fig.1-4 show the RMSE averaged 60 experiments obtained by these methods with sine type and sigmoidal type hidden nodes. It can be seen that CB-ELM can obtain much better generalization performance than other methods when a sigmoidal/sine hidden node is used. In practical applications, the residual error of neural network reduces very slowly and that will lead to neural network growing procedure stop, but CB-ELM can reach expected learning accuracy at early learning stage.

Table 1: Specification of 8 benchmark data sets

Datasets	Type	Attribution	Training datasets	Testing datasets
Air Quality	Regression	15	5358	4000
Bike Sharing Dataset	Regression	16	9389	8000
Communities and Crime	Regression	128	1000	994
Cuff-Less Blood Pressure Estimation	Regression	3	7000	5000
Geographical Original of Music	Regression	68	559	500
NoisyOffice	Regression	216	110	106
Online News Popularity	Regression	61	20000	19797
Parkinsons Telemonitoring	Regression	26	3800	2075

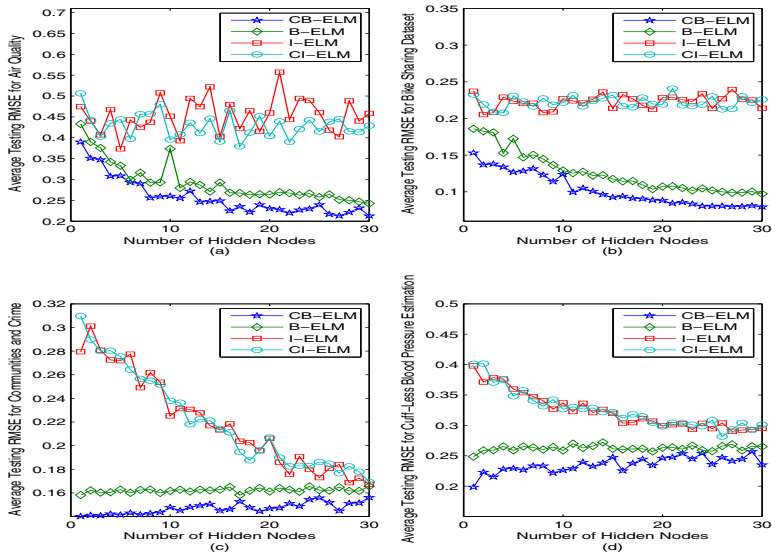

Figure 1: Testing RMES of different algorithms with sine hidden nodes in Air Quality, Bike Sharing Dataset, Communities and Crime and Cuff-Less Blood Pressure Estimation

3.2. Acquiring greenhouse data

Experimental data are derived from the solar greenhouse of The Institution Vegetable and Fruit of Chinese Academy of Agricultural Sciences, which is located in 40° 07', 116° 09'. Area of the solar greenhouse with geometric dimensions (length = 50m; width = 6.4m; height of ridge = 3.24m) is 300 m^2. The north wall is a layered structure 0.6m thick constructed of brick, foam insulation and an air layer. The roof is covered by a 0.12 mm thick plastic and a 22 mm thick thermal insulting blanket laid over the roof each night in winter. Tomato is planted in the solar greenhouse. The cross-section of the solar greenhouse structure and sensor positions inside the solar greenhouse are shown in Fig.5.

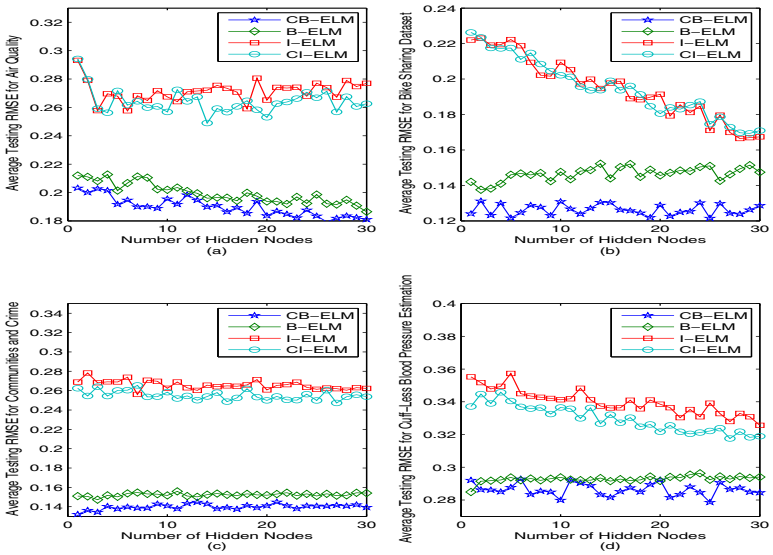

Figure 2: Testing RMES of different algorithms with sigmoidal hidden nodes in Air Quality, Bike Sharing Dataset, Communities and Crime and Cuff-Less Blood Pressure Estimation

During the experiment, the data acquisition system recorded the solar radiation(HA2003, valid solar radiation range of 200 to 200000 lux, with precision of ±7%), wind speed(NZ-FS, valid wind speed range of 0m/s to 32.4m/s, with precision of ±1 m/s), inside and outside the solar greenhouse temperature and humidity(SHT10, valid temperature range of -40°C to 123.8°C, with precision of ±0.5°C; valid humidity range of 0% to 100%, with precision of ±5%). The database was taken from 00:00 January 10th to 00:00 January 23th in 2015. It consists of 1872 sets of data(the sampling time is ten minutes). Fig.6 represents the collected data in the solar greenhouse. The thermal insulting blanket is rolled up at 9:00 and rolled down at 15:00.

Outside temperature, outside humidity, solar radiation and wind speed are the main influencing factors of the solar greenhouse humidity and temperature. The four main influencing factors and previous inside humidity and inside temperature form the input vector of the prediction model, as shown in Fig.7.

3.3. Prediction results of solar greenhouse environment model

To analyse the prediction performance of model based on CB-ELM, SVM, BP, RBF and B-ELM are selected for comparison. According to the conclusion in 2.2, the paper adopts sigmoidal activation function for B-ELM and CB-ELM, the number of hidden nodes for B-ELM and CB-ELM is 2. RBF neural network uses Gaussian function as the radial basis function. The paper adopts

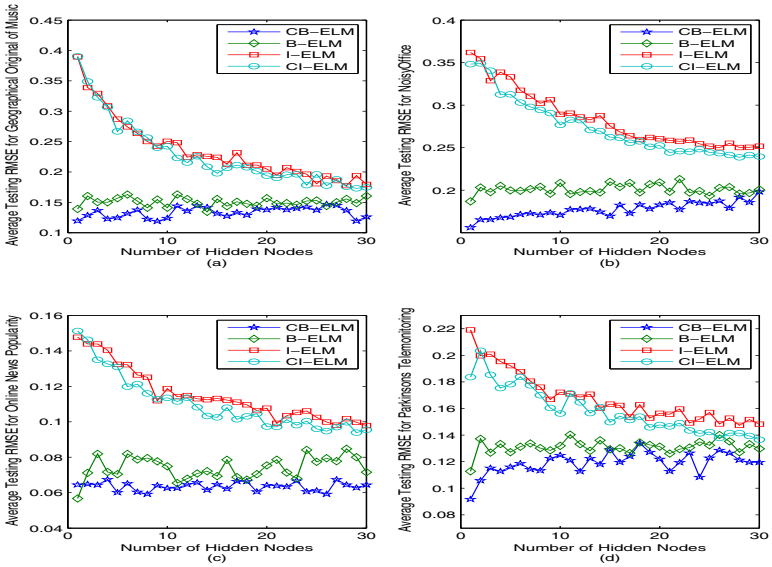

Figure 3: Testing RMES of different algorithms with sine hidden nodes in Geographical Original of Music, NoisyOffice, Online News Popularity and Parkinsons Telemonitoring

sigmoidal activation function for BP, the number of hidden nodes for BP is 20, and BP neural network includes one hidden layer. In this paper, we choose the RBF kernel (the width of the kernel is 9) as the kernel function of SVM. The performance indexes are calculated from the following equations:

$$RMSE = \sqrt{\frac{\sum_{i=1}^{N}(y_i - \hat{y}_i)^2}{N}} \tag{33}$$

$$MV = 1 - \frac{\sum_{i=1}^{N}(y_i - \hat{y}_i)^2}{\sum_{i=1}^{N}(y_i - \bar{y}_i)^2} \tag{34}$$

Where y_i is the output of a predicting model, $\hat{y}_i$ is world value, $\bar{y}_i$ is average of world value, N is number of sample.

The indexes root mean square error (RMSE) and model validity (MV) shown in Tab 2 are used to evaluate the predicting capacity of models based on CB-ELM, SVM, BP, RBF and B-ELM. The test data fitting curve and predicted error curve based on CB-ELM, SVM, BP, RBF and B-ELM are shown in Fig.8-14. In BP, the temperature measurement error range was [-9.3884°C, 7.3089°C], humidity testing error range was [-11.1974%, 25.022%]. In RBF, the temperature measurement error range was [-12.3965°C, 15.4553°C], humidity testing error range was [-29.0195%, 21.8348%]. In SVM, the tem-

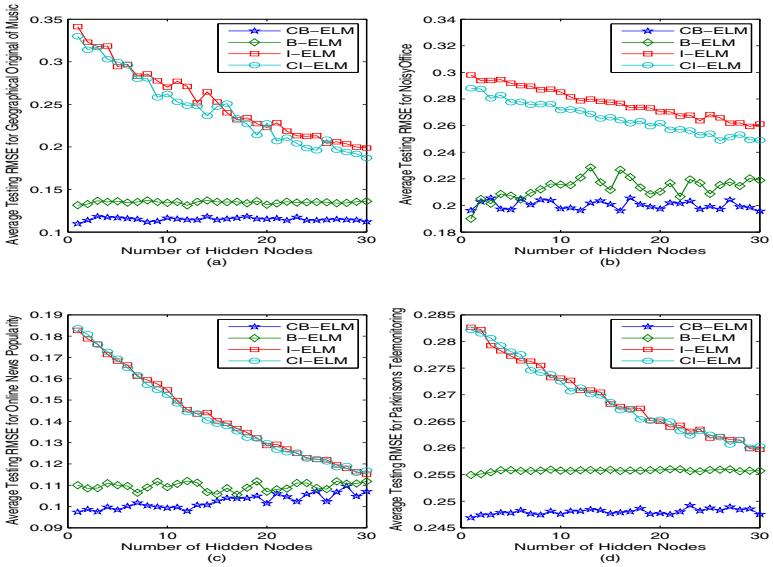

Figure 4: Testing RMES of different algorithms with sigmoidal hidden nodes in Geographical Original of Music, NoisyOffice, Online News Popularity and Parkinsons Telemonitoring

perature measurement error range was [-7.7105°C, 6.1242°C], humidity testing error range was [-12.5948%, 16.4016%]. In B-ELM, the temperature measurement error range was [-8.4898°C, 6.6051°C], humidity testing error range was [-13.4115%, 18.7169%]. In CB-ELM, the temperature measurement error range was [-6.2279°C, 5.9264°C], humidity testing error range was [-13.2306%, 14.7741%].

Compared with BP, RBF, SVM and B-ELM, the prediction results of CB-ELM show that root mean square error of temperature is reduced by 1.2757°C, 2.5626°C, 1.3389°C, 1.2579°C, root mean square error of of humidity is 2.2616%, 3.9578% 2.0522%, 2.329%, and model validity of temperature and humidity are improved by 0.0622, 0.1464, 0.0787, 0.0515 and 0.1206, 0.2443, 0.0995, 0.0653 respectively, so the CB-ELM is more effective, and it has certain reference value for intelligent control of the solar greenhouse microclimate.

4. Conclusion

In this paper, an improved learning algorithm called convex bidirectional extreme learning machine (CB-ELM) is presented. Different from B-ELM, based on a convex optimization method, CB-ELM recalculates the output weights of the existing hidden nodes after a new hidden node is added. CB-ELM can obtain a faster convergence rate and more compact network architecture while

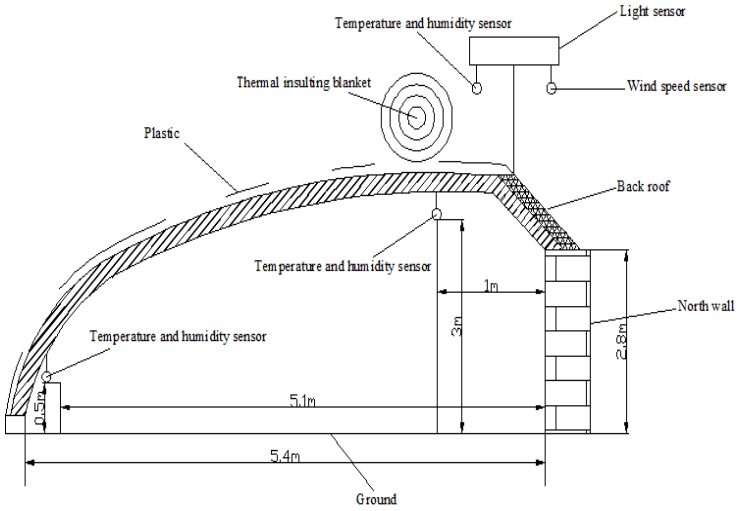

Figure 5: Schematic diagram of the solar greenhouses and sensor positions

Table 2: Comparison result of different prediction methods

Model	Temperature		Humidity	
	Root mean square error /°C	Model validity	Root mean square error/%	Model validity
BP	2.7166	0.9104	4.7604	0.8478
RBF	4.0035	0.8262	6.4566	0.7241
SVM	2.7798	0.8939	4.5510	0.8689
B-ELM	2.6988	0.9211	4.8278	0.9031
CB-ELM	1.4409	0.9726	2.4988	0.9684

retaining the simplicity and efficiency of IELM. CB-ELM is verified through the experiment of predicting solar greenhouse temperature and humidity using real-world data.

References

References

[1] X. Zhang, H. L. wang, Z. R. Zou, and S. J. Wang, 'CFD and weighted entropy based simulation and optimisation of Chinese Solar Greenhouse temperature distribution', Biosystems Engineering, 142 (2016), 12-26.

[2] M. Taki, Y. Ajabshirchi, S. F. Ranjbar, A. Rohani, and M. Matloobi, 'Heat transfer and MLP neural network models to predict inside environment

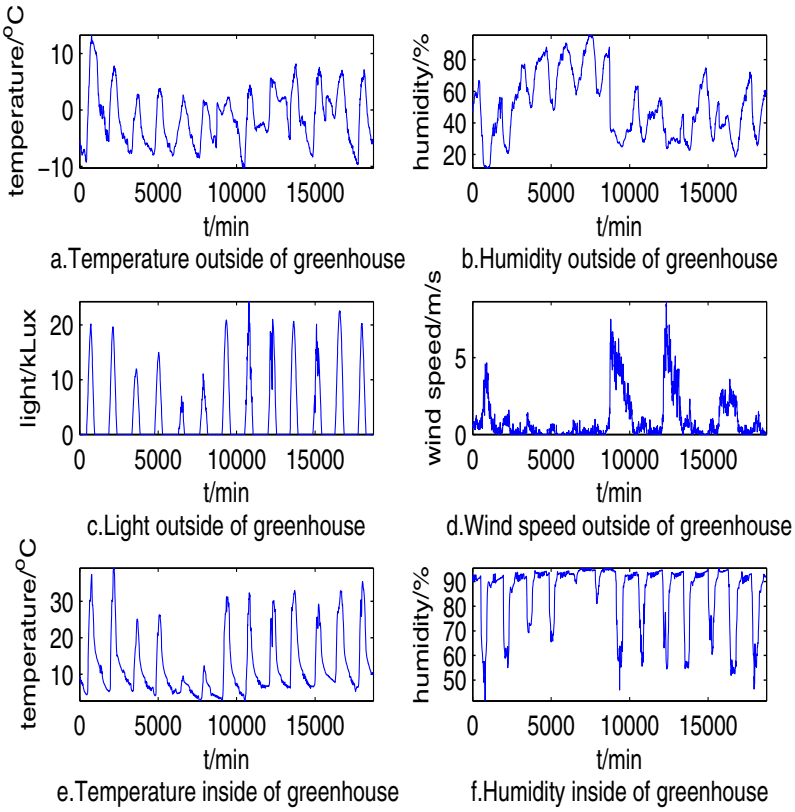

Figure 6: Variation of temperature and humidity inside greenhouse, temperature, humidity, light and wind speed outside greenhouse

variables and energy lost in a semi-solar greenhouse', Energy And Buildings, 110 (2016), 314-329.

[3] M. Taki, Y. Ajabshirchi, S. F. Ranjbar, A. Rohani, and M. Matloobi, 'Modeling and experimental validation of heat transfer and energy consumption in an innovative', Information Processing in Agriculture, 3 (3) (2016), 157-174.

[4] H. H. Yu, Y. Y. Chen, S. G. Hassan, D. L. Li, 'Prediction of the temperature in a Chinese solar greenhouse based on LSSVM optimized by improved PSO', Computers and Electronics in Agriculture, 122 (2016), 94-102.

[5] H. G. Mobtaker, Y. Ajabshirchi, S. F. Ranjbar, M. Matloobi, 'Solar energy conservation in greenhouse: Thermal analysis and experimental validation', Renewable Energy, 96 (1) (2016), 509-519.

[6] L. D. Albright, R. S. Gates, K. G. Arvanities, A. E. Drysdale. Environmental control for plants on earth and in space[J]. IEEE Control System

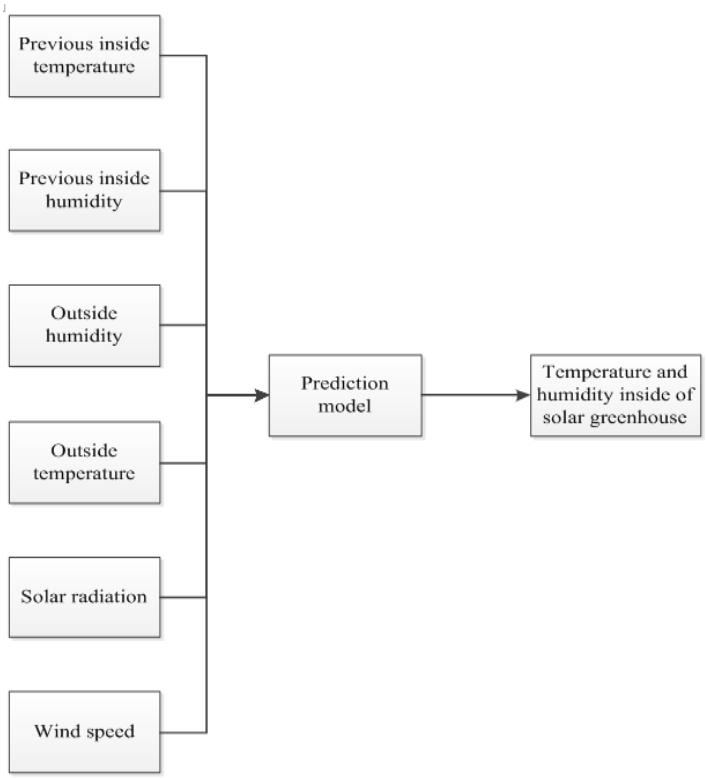

Figure 7: Building up the training sets of the prediction model

Magazine, 21 (5) (2001), 28-47.

[7] P. M. Ferreira, E. A. Faria, and A. E. Ruano, 'Neural Network Models in Greenhouse Air Temperature Prediction', Neurocomputing, 43 (2002), 51-75.

[8] F. He, C. W. Ma, 'Modeling Greenhouse Air Humidity by Means of Artificial Neural Network and Principal Component Analysis', Computers and Electronics in Agriculture, 71 (2010), S19-S23.

[9] F. Fourati, 'Multiple Neural Control of a Greenhouse', Neurocomputing, 139 (2014), 138-144.

[10] D. C. Wang, M. H. Wang, and X. J. Qiao, 'Support Vector Machines Regression and Modeling of Greenhouse Environment', Computers And Electronics In Agriculture, 66 (1) (2009), 46-52.

[11] A. Trabelsi, F. Lafont, M. Kamoun, and G. Enea, 'Fuzzy Identification of a Greenhouse', Applied Soft Computing, 7 (3) (2007), 1092-1101.

[12] F. He, W. C. Ma, 'Greenhouse Air Humidity Modeling Based on Principal

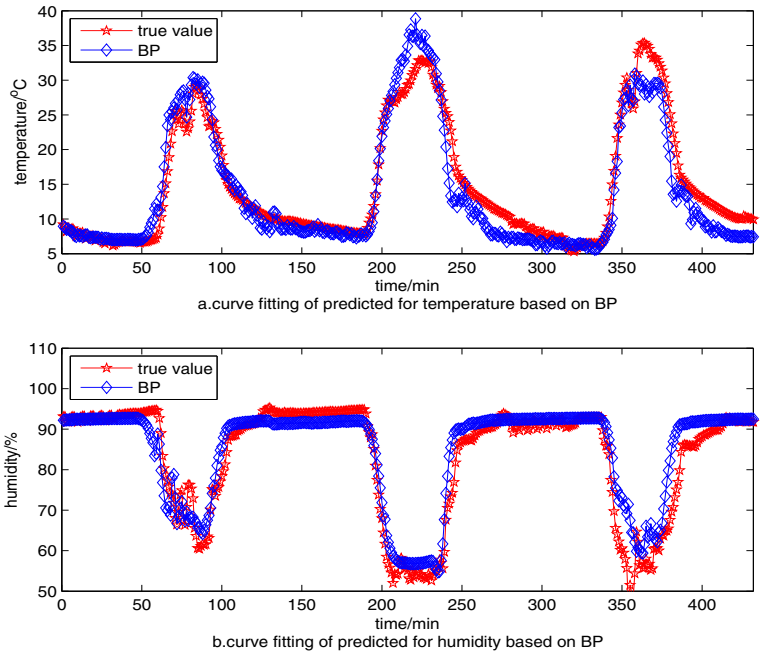

Figure 8: Predicted curve for temperature and humidity in solar greenhouse based on BP

component Analysis and Artificial Neural Network', Journal of Shanghai Jiaotong University (Agricultural Science), 26 (5) (2008), 428-431.

[13] Y. T. Xu, L. Wang, B. X. Zhang, L. C. Chen, H. Xu and C. Y. Zhou, 'Application of RBF Neural Network in Humidity Simulation and Prediction of Northern Sunlight Greenhouse', Journal of Shenyang Agricultural University, 45 (6) (2014), 726-730.

[14] D. Guo, Y. Zhang, Z. Xiao, Mao M., and J. Liu, 'Common Nature of Learning between Bp-Type and Hopfield-Type Neural Networks', Neurocomputing, 167 (2015), 578-586.

[15] X. X. Qi, Z. H. Yuan, and X. W. Han, 'Diagnosis of Misalignment Faults by Tacholess Order Tracking Analysis and RBF Networks', Neurocomputing, 169 (2015), 439-448.

[16] S. Ekici, S. Yildirim, and M. Poyraz, 'A Transmission Line Fault Locator Based on Elman Recurrent Networks', Applied Soft Computing, 9 (1) (2009), 341-347.

[17] G. B. Huang, L. Chen, and C. K. Siew, 'Universal Approximation Using Incremental Constructive Feedforward Networks with Random Hidden Nodes', Ieee Transactions on Neural Networks, 17 (4) (2006), 879-892.

[18] G. B. Huang, L. Chen, 'Convex Incremental Extreme Learning Machine', Neurocomputing, 70 (16-18) (2007), 3056-3062.

[19] G. B. Huang, L. Chen, 'Enhanced Random Search Based Incremental Extreme Learning Machine', Neurocomputing, 71 (16-18) (2008), 3460-3468.

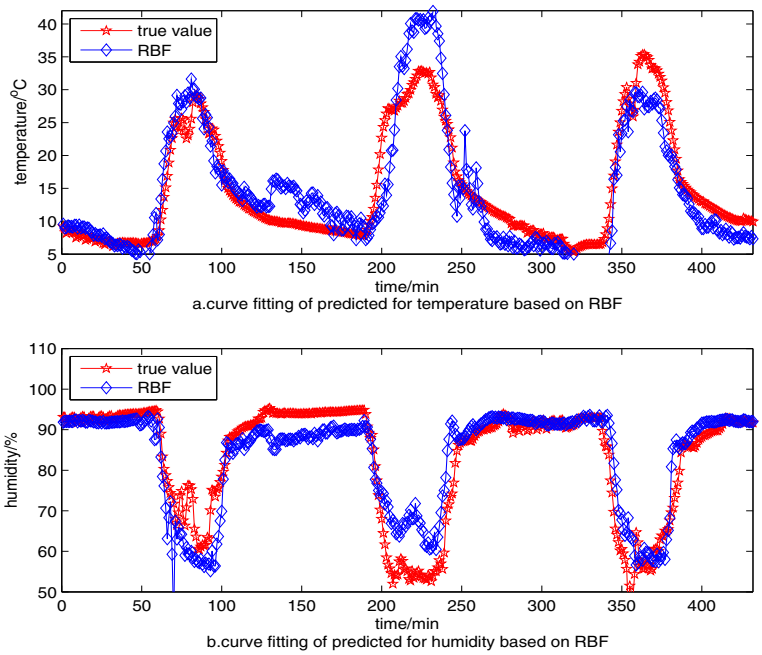

Figure 9: Predicted curve for temperature and humidity in solar greenhouse based on RBF

[20] Y. Lan, Y. C. Soh, and G. B. Huang, 'Two-Stage Extreme Learning Machine for Regression', Neurocomputing, 73 (1) (2010), 3028-3038.

[21] G. Feng, G. B. Huang, Q. Lin, and R. Gay, 'Error Minimized Extreme Learning Machine with Growth of Hidden Nodes and Incremental Learning', IEEE Trans Neural Netw, 20 (8) (2009), 1352-1357.

[22] Y. Lan, Y. C. Soh, and G. B. Huang. 'Two-stage extreme learning machine for regression'. Neurocomputing, 73 (16-18) (2010) 3028-3038.

[23] Y. Yang, Y. Wang, and X. Yuan, 'Bidirectional Extreme Learning Machine for Regression Problem and Its Learning Effectiveness', IEEE Trans Neural Netw Learn Syst, 23 (9) (2012), 1498-1505.

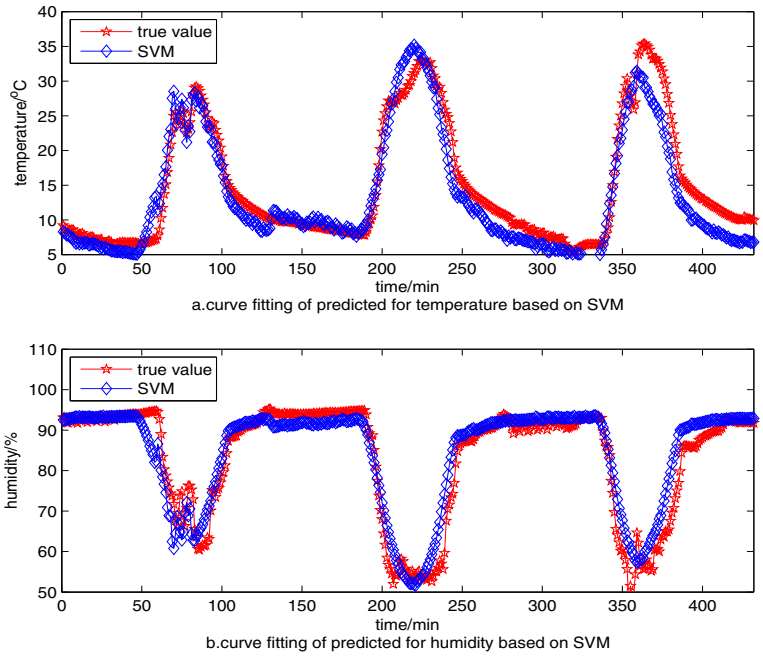

Figure 10: Predicted curve for temperature and humidity in solar greenhouse based on SVM

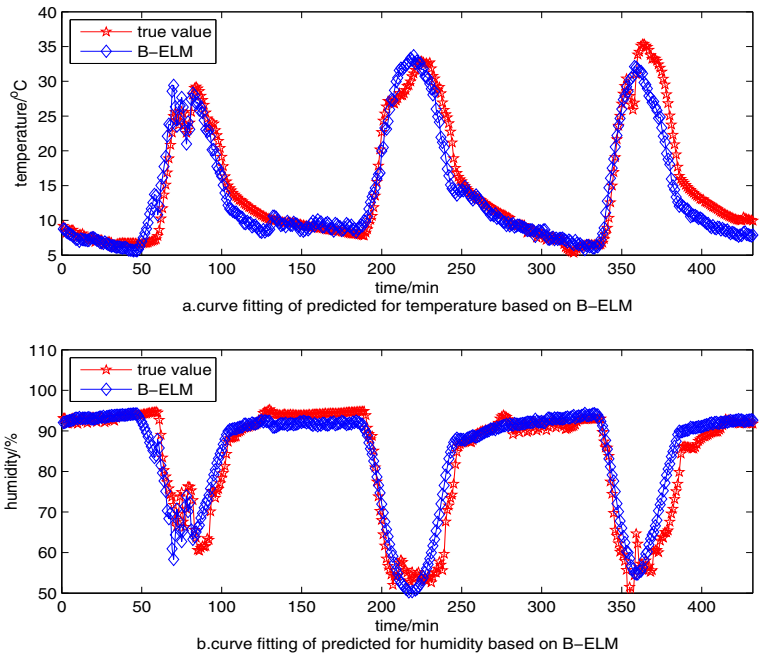

Figure 11: Predicted curve for temperature and humidity in solar greenhouse based on B-ELM

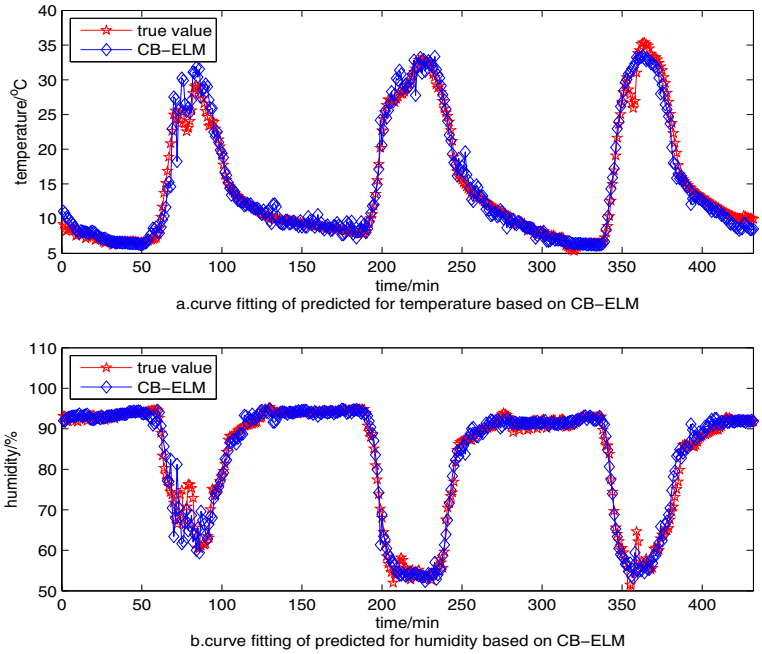

Figure 12: Predicted curve for temperature and humidity in solar greenhouse based on CB-ELM

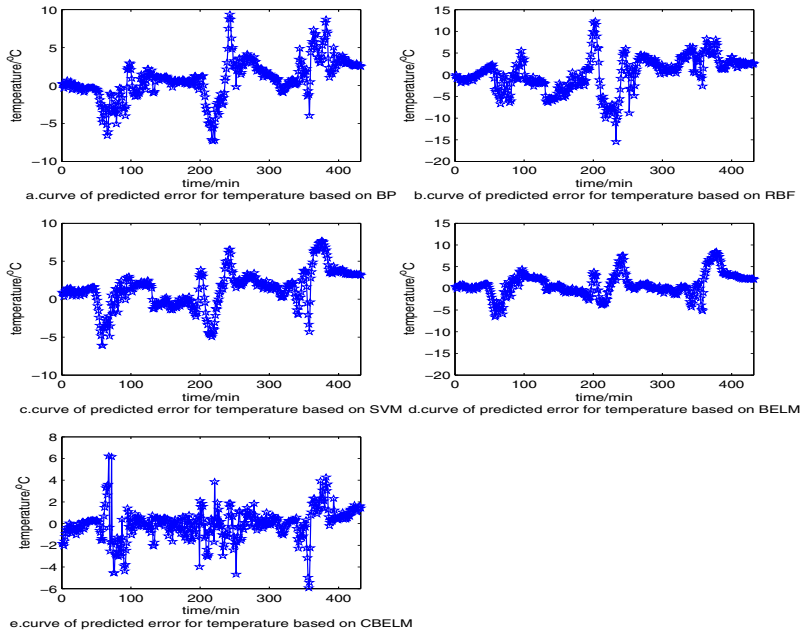

Figure 13: Predicted error curve for temperature in solar greenhouse based on five methods

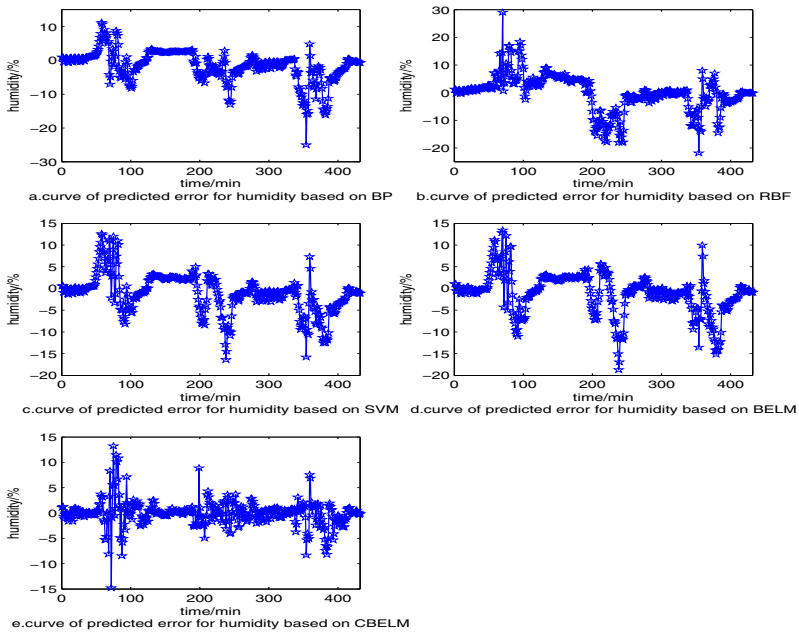

Figure 14: Predicted error curve for humidity in solar greenhouse based on five methods

Biography

Weidong Zou was born in Guangdong Province, China, in 1985.He received his M.S. degree in 2012 from the College of Information Science and Technology, Beijing University of Chemical Technology. He is currently pursuing PhD degree in Beijing Institute of Technology. His research interests include neural network, modeling and simulation of solar greenhouse.

Fenxi Yao was born in Hebei Province, China, in 1964.He received M.S. from Beijing Institute of Technology in 1987.He is a associate professor of School of Automation, Beijing Institute of Technology from 2000 - present. His research interests include industry automation, computer control system design and application.

Baihai Zhang was born in Shandong Province, China, in 1966. He received the Ph.D. degree from Harbin Institute of Technology, China, majoring fluid power transmission and control. Then he held a postdoctoral fellowship with School of Mechanical Engineering, Beijing Institute of Technology, China, from 1994 until 1997. He is a professor at School of Automation, Beijing Institute of Technology, from 2002 to present. He was a Senior Visiting Scholar at Michigan State University, USA, in 2001, and was a visiting scholar at University of the West of England, UK, in 2006. His current research interests include modeling and simulation of complex mechatronic systems, wireless sensor networks and multi-agent control systems.

Chaoxing He was born in 1965 in Shanxi Province, China. He is research scientist of Institute of Vegetables and Flowers, Chinese Academy of Agricul3 30 tural Sciences (CAAS). He got his Ph.D. from Institute of Botany, Chinese Academy of Sciences. From 1995 to 1997, He worked as assistant researcher in Institute of Crop Breeding and Cultivation, CAAS. Since 1997, Dr. He went to IVF, CAAS to study vegetable organic cultivation techniques and vegetable production expert decision system. More than 130 papers and 6 books had been 335 published until now. He was awarded the second National Prize for Progress in Science and Technology and Ministry Prize in Science and Technology three times.

Zixiao Guan was born in 1990 in Beijing, China. He received his B.S. degree in 2012 from the School of Automation, Beijing Institute of Technology. He is currently pursuing PhD degree in Beijing Institute of Technology. His research interests include mobile ad hoc networks, mobile computing, and localization algorithms for WSNs and MSNs.